DYNAMICS OF PHOTODISSOCIATION OF HONO AT 369 nm: MOTIONAL ANISOTROPY AND INTERNAL STATE DISTRIBUTION OF THE OH FRAGMENT

R. VASUDEV, R.N. ZARE
Department of Chemistry, Stanford University, Stanford, California 94305, USA

and

R.N. DIXON
School of Chemistry, University of Bristol, BS8 1TS, UK

Received 17 January 1983; in final form 8 February 1983

Anisotropic translational and rotational motion is observed in the ground-state hydroxyl radical generated by photolysis of *trans*-nitrous acid. The OH translational motion, determined from an analysis of Doppler line profiles, shows a sharply peaked velocity distribution with ≈46% of the total available energy (≈10300 cm^{-1}) appearing in OH recoil. The OH internal state distribution, determined from the laser excitation spectrum, is vibrationally and rotationally cold and the two $^2\Pi$ spin–orbit components are not in equilibrium. These results are compared with a simple impulse model for the fragmentation process.

1. Introduction

Molecular photofragmentation has long been regarded as a "half collision", where the recoiling fragments are prepared by photon impact [1,2]. As such, elucidation of the dynamics of fragmentation events is a prerequisite to the detailed understanding of collisional (reactive) processes. In a photofragmentation process the parent molecule is prepared spatially aligned in an excited internal state. The available energy then becomes partitioned into the internal degrees of freedom of the products and into their translational recoil. If the dissociation is faster than molecular rotation the alignment of the parent may result in rotational alignment of the products, and also in an anisotropic velocity distribution. Ideally, for each parent molecular state, one would like to measure the fragment yield as a function of all internal-state quantum numbers (v, L, S, J, M_J) as well as the translational motion. Such a study, especially the internal-state-dependent anisotropic velocity distribution, has not previously been carried out for molecular photofragments, although flash photolysis, time-of-flight fragment mass analysis, and photofragment polarized emission have made valuable contributions toward this general aim.

A powerful technique that is capable of providing the desired detailed information is the one based on Doppler spectroscopy of photo products [3] using a narrow band probe laser. Here we report such a study of OH produced by photolysis at 369 nm of *trans*-nitrous acid:

$$\mathrm{HONO}(\tilde{X}) + h\nu \rightarrow \mathrm{HONO}(\tilde{A}) \rightarrow \mathrm{OH}(X\,^2\Pi) + \mathrm{NO}(X\,^2\Pi). \quad (1)$$

The lowest energy transition in HONO(300–390 nm) has previously been assigned to the $\tilde{A}\,^1A''$–$\tilde{X}\,^1A'$ system, and is of the $\pi^* \leftarrow n$ type involving the –N=O chromophore [4]. This absorption spectrum consists of a progression (2_0^n) in the ν_2 vibration associated predominantly with the terminal NO stretch, suggesting that the only internal coordinate that undergoes an appreciable change is the N=O bond length. It has been shown that process (1) has unit quantum efficiency [5]. The bands are devoid of any discernible rotational structure, implying that the fragmentation of the $\tilde{A}$ state is probably faster than rotation. Thus this molecule is especially suitable for a study of anisotropic fragment motion.

2. Experimental

Nitrous acid is prepared by mixing H_2O vapor, NO_2 and NO in the ratio 1 : 2 : 1 at a total pressure of ≈50 Torr. These are allowed to stand overnight to establish the surface-catalyzed equilibrium [6]:

$$H_2O + NO_2 + NO \rightleftharpoons 2HNO_2 \, . \quad (2)$$

This mixture is slowly bled into the photolysis chamber at a pressure of 30–60 mTorr.

The photolysis frequency (27100 cm^{-1}) is generated by Raman shifting the second harmonic of the output of a Nd : YAG laser (Quanta-Ray DCR-1A) in H_2. The second anti-Stokes radiation, which excites the 2^1_0 band in *trans*-HONO, is isolated by a Pellin–Broca prism and passed through a polarizer. The probe beam is obtained by frequency doubling a N_2 laser-pumped dye laser (Molectron UV24/DL II). This is used to excite OH in the A–X (1,0) band (281–285 nm), which is monitored through emission of the (1,1) transition (310–330 nm). The two laser beams are counterpropagated through the photolysis chamber, with the probe arriving ⩽50 ns after the photolysis beam.

For comparison with the fragment spectrum the spectrum of thermalized (300 K) OH is recorded. For this purpose OH is generated by the reaction H + NO_2 → NO + OH and allowed to equilibrate collisionally.

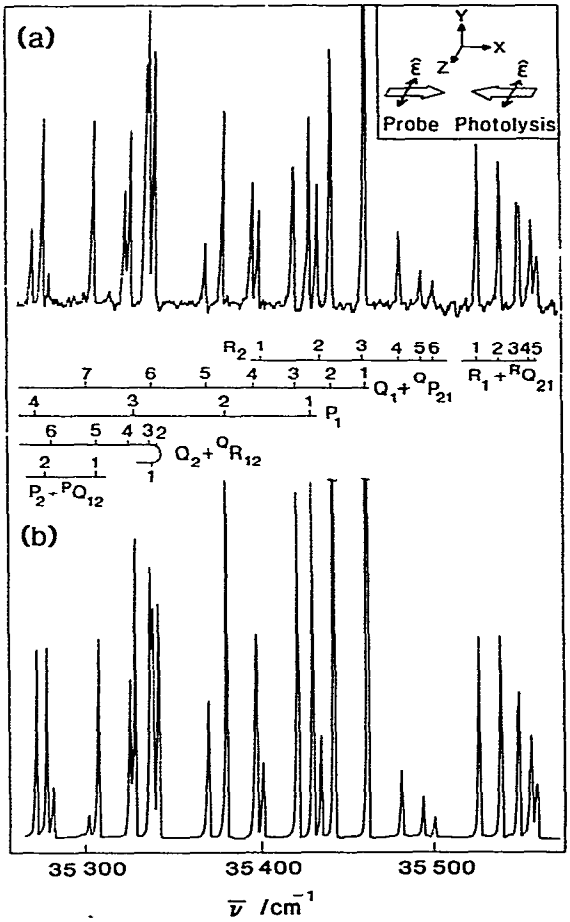

Fig. 1. Comparison of (a) the excitation spectrum of the $A\,^2\Sigma^+ - A\,^2\Pi$ (1,0) band of the OH fragment generated by 369 nm photolysis of HONO and (b) the excitation spectrum of thermalized (300 K) OH. The inset shows the photolysis/probe geometry: the two beams, polarized along the *Z* axis, are counterpropagated along the *X* axis. The photomultiplier, which detects all polarizations, is along the *Z* axis.

3. Results and discussion

Fig. 1a shows a portion of a broad band (1.3 cm^{-1}) $A\,^2\Sigma^+ - X\,^2\Pi$ excitation spectrum of the OH photofragment, along with the experimental photolysis/probe geometry (see inset). Shown in fig. 1b, for comparison, is the excitation spectrum of the thermalized OH. The most striking difference between these spectra is the intensity ratio between the branches originating from the F_2'' levels ($J'' = N'' - \frac{1}{2}$) and the F_1'' levels ($J'' = N'' + \frac{1}{2}$). This ratio is much larger in the fragment OH spectrum (fig. 1a) than in the thermalized OH spectrum (fig. 1b), as readily seen by comparing, for example, the R_2 and P_1 line intensities in the two spectra. Thus the F_2 levels are preferentially populated. Fig. 2 shows Boltzmann plots constructed for the observed intensities, corrected for polarization effects, and the published OH A–X line strength factors [7]. The "effective temperatures" from these plots are 320 K for the $F_1(N)$ levels and 275 K for the $F_2(N)$ levels. In addition to being rotationally not hot, the OH fragment is also vibrationally cold, since the A–X (2,1) band could not be detected.

The next striking aspect of the fragment excitation

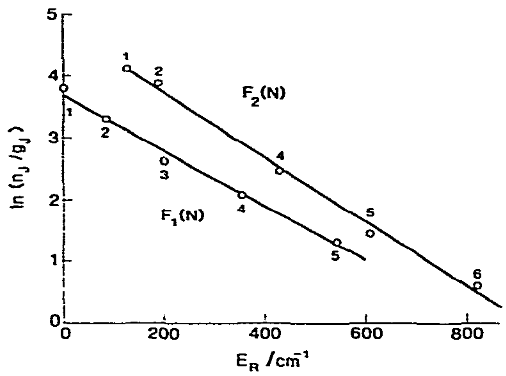

Fig. 2. Boltzmann plots of the relative populations of the $F_1''(J'' = N'' + \frac{1}{2})$ and $F_2''(J'' = N'' - \frac{1}{2})$ levels of the OH fragment.

spectrum concerns the rotational alignment of the OH photoproduct. For the case presented in fig. 1a the probe and photolysis electric vectors are along the Z axis. Spectra are also recorded in which the parent transition moment is preferentially aligned along the Y axis by rotating the photolysis polarization vector. When this is done, the relative intensities of the higher members of the Q branches are lowered, by a factor of approximately two for the highest observed $N''[Q_2(6)]$. The P and R branches, on the ohter hand, show the opposite behavior in accord with the theory of LIF-probed rotational alignment [8]. We thus conclude that the fragment rotational axis is preferentially aligned parallel to the photolysis polarization vector, and hence parallel to the electronic transition moment in the parent molecule. Quantitative measurements of such alignment effects will be presented in a later paper.

The third important measurement in the present experiments concerns the translational motion of the OH fragment. The photolysis photon energy is ≈1.24 eV in excess of the HO–NO bond dissociation energy [6,9]. Since the OH fragment is vibrationally and rotationally cold a substantial portion of the available energy might be expected to be channeled into translation. In addition, the translational motion is anticipated to be anisotropic, as mentioned earlier. In the current experiments this motion is probed by measuring the shapes of selected lines with the probe laser bandwidth narrowed to ≈0.1 cm^{-1}. All the probed lines show a similar double-peaked shape, which we call a split Doppler profile, indicating that there are more fragments moving forward and backward with high velocity than those with low velocity along the probe laser propagation axis (the X axis: see fig. 1). Since this axis is perpendicular to the parent molecule alignment axis (the Z axis), the observed distribution corresponds to anisotropic OH translation predominantly in the XY plane. This appears to be the first observation of a Doppler split line profile of a *molecular* photofragment; however, such profiles have been observed for the H atom both in photodissociation [10] and in electron impact dissociation [11]. Doppler spectroscopy of molecular photofragments has previously been applied to NH_2 and OH produced by the infrared multiphoton dissociation of CH_3NH_2 [12] and CH_3OH [13] but the line profiles were not observed to be split. Doppler spectroscopy has also been applied to the OH(OD) product of the chemical reaction $H(D) + NO_2 \rightarrow OH(OD) + NO$, but again the line shapes are approximately gaussian [14].

From the theory of Zare and Herschbach [3], adapted to our experiment, the expected lineshape for a single fragment velocity v is

$$S(\Delta\bar{\nu}_0) = (1/\Delta\bar{\nu}_D)[1 - \tfrac{1}{2}\beta P_2(\Delta\bar{\nu}_0/\Delta\bar{\nu}_D)] , \qquad (3)$$

where $\Delta\bar{\nu}_0$ is the displacement from the line-center and $\Delta\bar{\nu}_D = \bar{\nu}_0 v/c$ is the Doppler shift. The anisotropy parameter β is equal to +2 or −1 in the limits of fragment recoil along, or perpendicular to, the parent molecule transition moment. This lineshape is depicted in fig. 3a for $\beta = -1$. A convolution of $S(\Delta\bar{\nu}_0)$ with a gaussian center-of-mass motion (fwhm = 0.063 cm^{-1}), a time-averaged gaussian laser profile (fwhm = 0.116 cm^{-1}), and a width $2\Delta\bar{\nu}_D = 0.61$ cm^{-1} is compared in fig. 3b with the observed $P_1(1)$ line profile. The above value of $2\Delta\bar{\nu}_D$ gives the best agreement between the fwhm of the simulated and the observed line profiles. Experimentally, all the lines are found to have almost the same width (0.63 ± 0.02 cm^{-1}) with a slight variation in the contrast of the central dip.

The satisfactory agreement between the simulated and experimental profiles shows that the β parameter must be close to the limiting value of −1, and that the velocity distribution must be sharply peaked. The value of $2\Delta\bar{\nu}_D = 0.61 \pm 0.01$ cm^{-1} corresponds to an OH fragment velocity of 2.58 km/s, equivalent to a translational energy of 4720 cm^{-1}. This is 46 percent of the total energy (10290 ± 200 cm^{-1}) available to the fragments. Conservation of linear momen-

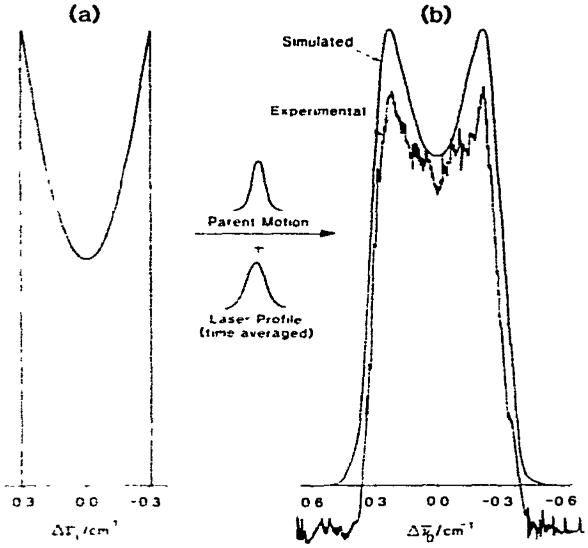

Fig. 3. The Doppler lineshape (a) calculated from $S(\Delta\bar{\nu}_0)$ using eq. (3) with $\beta = -1$ and $2\Delta\bar{\nu}_D = 0.61\ \mathrm{cm}^{-1}$, and (b) obtained by convoluting $S(\Delta\bar{\nu}_0)$ with 300 K thermal HONO motion (fwhm = 0.063 cm^{-1}) and a time-averaged gaussian laser profile (fwhm = 0.116 cm^{-1}), deduced from the thermalized OH lineshapes. Shown along with the simulated profile is the experimental OH photofragment $P_1(1)$ lineshape.

tum then implies the presence of 2680 cm^{-1} in NO translation. Thus a high percentage of the available energy (72%) appears in fragment recoil.

Finally, we compare our result with that predicted by a simple impulse model [15] in which a short-range repulsive force acts along the central O–N bond axis between rigid OH and NO groups. This leads to a partition between translational and rotational energy according to

$$E_T(\mathrm{OH}) : E_T(\mathrm{NO}) : E_R(\mathrm{OH}) : E_R(\mathrm{NO})$$

$$= m_N m_O m_{NO} : m_N m_O m_{OH} : m_N m_{NO} m_H \sin^2\theta_{HON}$$

$$: m_O^2 m_{OH} \sin^2\theta_{ONO} . \qquad (4)$$

With the ground-state inter-bond angles ($\theta_{HON} = 105°$, $\theta_{ONO} = 120°$), this partitioning of the available energy gives

$$E_T(\mathrm{OH}) = 4840\ \mathrm{cm}^{-1}, \quad E_T(\mathrm{NO}) = 2740\ \mathrm{cm}^{-1},$$

$$E_R(\mathrm{OH}) = 280\ \mathrm{cm}^{-1}, \quad E_R(\mathrm{NO}) = 2440\ \mathrm{cm}^{-1}. \qquad (5)$$

This model correctly accounts for the high translational and low rotational excitation observed for OH. However, the "available energy" used in the above calculation includes the vibrational quantum initially deposited in the terminal NO bond. The photolysis of HONO in different members of the 2_0^n progression will provide a test for the validity of this non-adiabatic assumption. Results of such further experiments will be reported elsewhere.

Acknowledgement

We thank the San Francisco Laser Center for the loan of a Nd : YAG laser. RND and RNZ are also grateful for the award of a NATO Grant (141.82) for International Collaboration. RNZ acknowledges the US National Science Foundation and the Shell Companies Foundation, Inc., for support through the Shell Distinguished Chairs Program.

References

[1] K.R. Wilson, in: Excited state chemistry, ed. J.N. Pitts (Gordon and Breach, New York, 1970).
[2] J.P. Simons, Specialist Periodical Report, Gas Kinetics and Energy Transfer, Vol. 2 (Chem. Soc., London, 1977) p. 56.
[3] R.N. Zare and D.R. Herschbach, Proc. IEEE 51 (1963) 173.
[4] G.W. King and D. Moule, Can. J. Chem. 40 (1962) 2057;
R.C. Mitchell and J.P. Simons, Discussions Faraday Soc. 44 (1967) 208.
[5] R.A. Cox and R.G. Derwent, J. Photochem. 6 (1976/7) 23.
[6] R. Varma and R.F. Curl, J. Phys. Chem. 82 (1976) 402.
[7] I.L. Chidsey and D.R. Crosley, J. Quant. Spectry. Radiative Transfer 23 (1980) 187.
[8] C.H. Greene and R.N. Zare, to be published.
[9] D.R. Stoll and H. Prophet, eds., JANAF Thermodynamic Tables, 2nd Ed., NSRDS-NBS 37 (1971).
[10] R. Schmiedl, H. Dugan, W. Meier and K.H. Welge, Z. Physik A304 (1982) 137.
[11] N. Kouchi, K. Ito, Y. Hatano and N. Oda, Chem. Phys. 70 (1982) 105, and references therein.
[12] R. Schmiedl, R. Boettner, H. Zacharias, U. Meier and K.H. Welge, Opt. Commun. 31 (1979) 329.
[13] R. Schmiedl, U. Meier and K.H. Welge, Chem. Phys. Letters 80 (1981) 495.
[14] E.J. Murphy, J.H. Brophy and J.L. Kinsey, J. Chem. Phys. 74 (1981) 331.
[15] A.F. Tuck, J. Chem. Soc. Faraday Trans. 2 (1977) 689.